

Article

# NiPd Supported on Mesostructured Silica Nanoparticle as Efficient Anode Electrocatalyst for Methanol Electrooxidation in Alkaline Media

Muliani Mansor <sup>1</sup>, Sharifah Najihah Timmiati <sup>1,\*</sup>, Wai Yin Wong <sup>1</sup> , Azran Mohd Zainoodin <sup>1</sup>, Kean Long Lim <sup>1</sup> and Siti Kartom Kamarudin <sup>1,2</sup>

<sup>1</sup> Fuel Cell Institute, Universiti Kebangsaan Malaysia, UKM Bangi 43600, Selangor, Malaysia; mulianimansor@yahoo.com (M.M.); waiyin.wong@ukm.edu.my (W.Y.W.); azrans@ukm.edu.my (A.M.Z.); kllim@ukm.edu.my (K.L.L.); ctie@ukm.edu.my (S.K.K.)

<sup>2</sup> Department of Chemical and Process Engineering, Faculty of Engineering and Built Environment, Universiti Kebangsaan Malaysia, UKM Bangi 43600, Selangor, Malaysia

\* Correspondence: najihah@ukm.edu.my; Tel.: +603-8911-8526; Fax: +603-8911-8530

Received: 28 September 2020; Accepted: 20 October 2020; Published: 25 October 2020



**Abstract:** The direct methanol fuel cell (DMFC) is a portable device and has the potential to produce 10 times higher energy density than lithium-ion rechargeable batteries. It is essential to build efficient methanol electrooxidation reaction electrocatalysts for DMFCs to achieve their practical application in future energy storage and conversion. A catalyst consisting of nickel–palladium supported onto mesostructured silica nanoparticles (NiPd–MSN) was synthesized by the wet impregnation method, while MSN was synthesized using the sol-gel method. MSN act as a catalyst support and has very good characteristics for practical support due to its large surface area (>1000 m<sup>2</sup>/g) and good chemical and mechanical stability. The microstructure and catalytic activity of the electrocatalysts were analyzed by X-ray diffraction (XRD), Fourier transform infrared (FTIR), field emission scanning electron microscopy (FESEM), Brunauer–Emmet–Teller (BET) theory, X-ray photoelectron spectroscopy (XPS), cyclic voltammetry (CV), and chronoamperometry (CA). XRD showed that the NiPd–MSN electrocatalysts had a high crystallinity of PdO and NiO, while FESEM displayed that NiPd was dispersed homogeneously onto the high surface area of MSN. In alkaline media, the catalytic activity toward the methanol oxidation reaction (MOR) of NiPd–MSN demonstrated the highest, which was 657.03 mA mg<sup>−1</sup> more than the other electrocatalysts. After 3600 s of CA analysis at −0.2 V (vs. Ag/AgCl), the MOR mass activity of NiPd–MSN in alkaline media was retained at a higher mass activity of 190.8 mA mg<sup>−1</sup> while the other electrocatalyst was significantly lower than that. This electrocatalyst is a promising anode material toward MOR in alkaline media.

**Keywords:** methanol oxidation reaction; alkaline medium; electrocatalyst; nickel; mesostructured silica nanoparticles

## 1. Introduction

The direct methanol fuel cell (DMFC) is acknowledged as the optimal fuel cell system considering that it can generate electricity by converting the methanol fuel directly at the fuel cell anode. As a promising source of power, it has also attracted great interest as it has clean, novel, low pollutant issuers, and noiseless sources of electricity [1]. Currently, substantial works have focused on investigating the electro-oxidation of methanol in electrolytes of high pH, alkaline. Alkaline electrolytes favored a reduction in methanol crossover, rapid kinetics, increased efficiency, and an extended choice of potential electrode materials, which allows cheaper metals to be used [2]. As previous studies have stated, acidic DMFC faces a significant problem, which is corrosion of the catalyst [3]. Alkaline DMFC is favorable

because it has good anodic kinetics of the methanol electro-oxidation reaction due to the weaker binding between the electrocatalyst and adsorbed carbonaceous intermediate species of methanol. Moreover, the reduction of methanol crossover from the anode to the cathode by electro-osmotic drag will result in high power densities in the single cell. Considering that the displacement of hydroxide ions takes place against the displacement of the alcohol in the anionic membranes exchange [4], hence, alkaline media can potentially be used in the DMFC as the electrolyte to replace acidic media.

Notably, Pt catalysts are recognized as one of the most desirable anode catalysts for the methanol oxidation reaction (MOR). Despite having high electrocatalytic activity toward MOR, its CO poisoning of the Pt active site and high cost impede the feasible commercialization of Pt catalysts in DMFCs [5,6]. Potentially, less costly metal catalysts like nickel, silver, and tin can replace the Pt catalysts. Nickel-based catalysts in alkaline media, compared to Pt catalysts, have sustained a lot of efforts in their development due to their surface oxidation properties [7]. The presence of surface oxidation Ni relatively enhances OH adsorption sites, which help to remove the oxidation of adsorbed CO during MOR [8]. In fact, in nature, nickel is more abundant and much cheaper than Pt. Apart from that, due to its high electrocatalytic activity toward MOR, palladium-based catalysts have been widely explored in the alkaline media. Notably, numerous studies have highlighted nickel with palladium catalysts as a replacement to Pt-based catalysts to obtain higher electrocatalytic activity towards MOR in alkaline media [9,10]. Additionally, several previous works of literature reported the capability of metal oxides as the electrocatalyst in MOR [11–15]. Wang et al. [14] studied the effect of oxides NiO and PdO as the anode electrocatalyst. It revealed that the existence of NiO and PdO in the electrocatalyst can improve catalytic activity, where NiO can enhance the anti-poison ability and provide an oxygen source for CO oxidation at lower potentials while PdO is an active species [16]. As discussed in previous research [17], Pt and Pt-based surface oxides can be categorized based on oxidation states as active and poison species. The Pt surface oxides with lower oxidation states (i.e., PtO, Pt(OH)<sub>2</sub>, and PtOH) are recognized as active species. They promote primary alcohol oxidation, whereas the Pt surface oxides with higher oxidation states (i.e., Pt(OH)<sub>3</sub> and PtO<sub>2</sub>) are poison species because they prevent alcohol oxidation. Ye et al. [15] reported the stability analysis for methanol oxidation on oxide (CeO<sub>2</sub>, NiO, Co<sub>3</sub>O<sub>4</sub>, and Mn<sub>3</sub>O<sub>4</sub>)-promoted Pd/C electrocatalysts. Pd–NiO/C produced the highest electrocatalytic activity compared to the other Pd-oxide/C; however, it is less stable in methanol oxidation. Calderon et al. [9] studied the catalytic activities toward MOR in an alkaline medium at different atomic ratios Pd:Ni (1:1 and 1:2) of PdNi/CB and reported that the PdNi/CB 1:2 electrocatalyst presented superior performance than PdNi/CB 1:1; and the catalytic performance was dependent on the ratio of the metal and promoter. According to a study by Tan et al. [18], PdNi was used to study the electrocatalytic activity toward ethanol electro-oxidation in an alkaline medium, and it showed great electrocatalytic activity (770.6 mA mg<sup>-1</sup>) and good stability. The addition of nickel could not only reduce the Pd loading; it is also believed that the oxophilicity of metals allows for the essential –OH group required for the oxidation of the adsorbed ethanol molecules.

To further improve the utilization of such catalysts, the choice of support materials is the crucial factor. Carbon-based materials such as carbon black, mesoporous carbon, carbon nanotubes, and graphene are broadly used supports. However, it is known that carbon-based materials under operating conditions undergo corrosion and electrochemical oxidation to produce surface oxides, and also CO/CO<sub>2</sub> [19]. The essential specifications of appropriate support for an electrocatalyst of the fuel cell in DMFC conditions are good electrical conductivity, high surface area, and adequate porosity to enable a good reactant flow and high chemical stability. Nowadays, mesostructured silica nanoparticles (MSN) have attracted substantial attention due to its properties of high surface area (>1000 m<sup>2</sup> g<sup>-1</sup>), good chemical and mechanical stability in terms of resistant to corrosion, and high porosity, which is suitable as catalyst support materials [20–22].

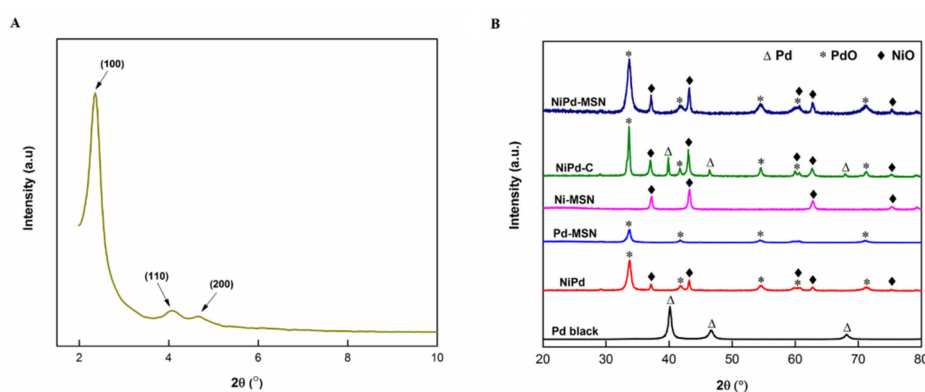
In this work, NiPd supported on MSN was synthesized by using the wet impregnation method. Despite this, NiPd catalysts for MOR have been extensively investigated, but to the best of our knowledge, these NiPd catalysts supported on MSN as the anode catalyst for MOR have not been

reported yet. To characterize the prepared electrocatalyst, X-ray diffraction (XRD), field emission scanning electron microscopy (FESEM), Fourier transform infrared (FTIR), X-ray photoelectron spectra (XPS), and Brunauer–Emmett–Teller (BET) were used, while cyclic voltammetry (CV), electrochemical surface area (ECSA), Tafel plot analysis, and chronoamperometry (CA) were used to evaluate electrocatalyst efficiency.

## 2. Results and Discussion

### 2.1. Structural Characterization

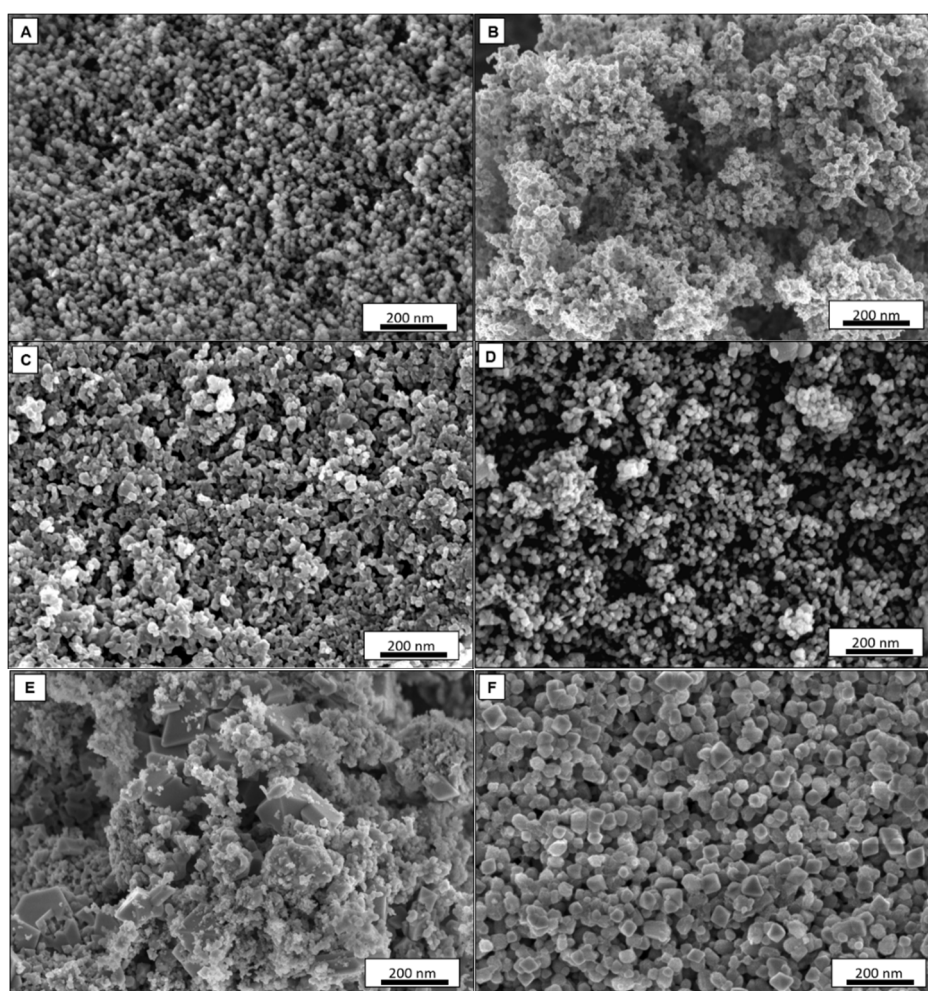
The X-ray diffraction (XRD) patterns of all the catalysts are displayed in Figure 1A,B. Figure 1A demonstrates the small-angle XRD pattern for the MSN in the range  $2\theta = 2\text{--}10^\circ$ . Noticeable peaks of diffraction were detected at  $2\theta = 2.33^\circ$ ,  $4.08^\circ$ , and  $4.70^\circ$  and are listed as (100), (110), and (200) reflections, respectively. The patterns demonstrated a diffraction peak shown in Figure 1A, which is listed to a p6mm hexagonal structure of mesoporous silica, displaying the high quality of the mesopore packing [23]. In all catalysts with MSN as support materials, as shown in Figure 1B, the diffraction peaks at  $2\theta = 37.2^\circ$ ,  $43.3^\circ$ ,  $62.8^\circ$ , and  $75.3^\circ$  were associated with the phase of NiO (JCPDS. 73-1519). The diffraction peaks at  $2\theta = 33.6^\circ$ ,  $54.6^\circ$ ,  $71.5^\circ$ , and  $79.3^\circ$  for the promoted catalysts could be ascribed to the PdO phase (JCPDS 00-041-1107). It is known only as an amorphous form of carbon; carbon black typically consists of near-spherical graphite particles [24]. For comparison, Pd black and NiPd–C nanoparticles were prepared. Pd black and NiPd–C catalysts showed diffraction peaks at the Bragg angles corresponding to the (111), (200), and (220) reflections of Pd at  $40.0^\circ$ ,  $46.8^\circ$ , and  $68.2^\circ$ , respectively. The experimental pattern was in agreement with the JCPDS No. 46-1043 standard crystallographic tables, indicating that the face-centered cubic (fcc) structure was Pd crystal. The previous research [14] revealed that the existence of NiO and PdO in the electrocatalysts could improve the performance of MOR. NiO can give an excellent catalytic activity for the dehydration reaction of methanol, while PdO in lower oxidation states act as an active species that can promote the oxidation of primary alcohols. This combination can lower the Pd poisoning possibility and enhance the chemical and electrochemical process equilibrium.



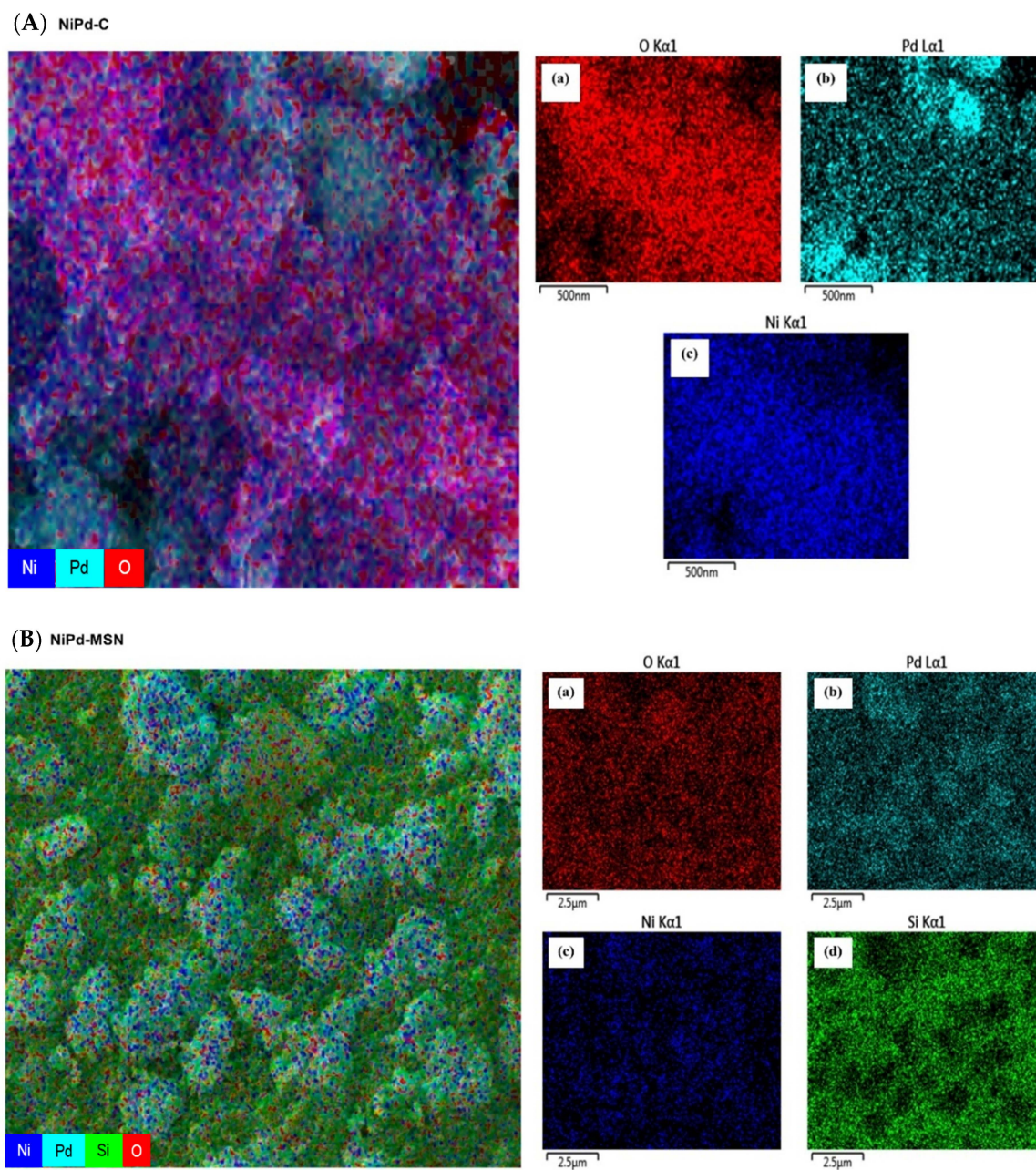
**Figure 1.** Small-angle (A) X-ray diffraction (XRD) patterns of MSN and wide-angle, (B) XRD patterns of Pd black, NiPd, Pd–MSN, Ni–MSN, NiPd–C, and NiPd–MSN electrocatalysts.

Figure 2A–F displays micrographs with the magnification of 30 kX for electrocatalysts of MSN, Pd black, Pd–MSN, Ni–MSN, NiPd–C, and NiPd–MSN, respectively. It can be seen that the spherical shape of the MSN was sustained with Ni, Pd, and NiPd loaded onto MSNs and the metal particles filled up some of the pores and were well-dispersed on the support of MSN powder. However, when the Ni, Pd, and NiPd were added, the shape of MSN was slightly reduced and less aggregated [21]. The bigger pore diameter of NiPd–MSN can be observed compared to bare MSN (Supplementary Materials Figure S1). The isomorphous substitution of nickel and palladium atoms into the silica frameworks may explain such great differences between nickel-containing and non-nickel samples.

This contributes to a large contraction of the walls and, as a result, the expansion of the pores [23]. Figure 2E is the NiPd catalyst deposited on the carbon black, NiPd-C; the FESEM image spotted several agglomerations of Ni and Pd nanoparticles. The dispersion of Ni and Pd nanoparticles can be seen through the mapping shown in Figure 3: (a) Ni and (b) Pd for both (A) NiPd-C and (B) NiPd-MSN electrocatalysts. From the mapping images of the NiPd-C electrocatalyst, both metals were evenly dispersed on the carbon black; but several agglomerations occurred for Pd. Additionally, from Figure 2E,F, it can be seen that both figures have different morphology, which in (E) is shown as the support. As mentioned in the XRD result (Figure 1A), MSN had a hexagonal structure. The NiPd-MSN electrocatalyst displayed the significant dispersion of NiPd metal on the surface of MSN, in agreement with the TEM image of the NiPd loaded catalyst, as shown in Figure 4. The presence of well-resolved pores of MSN can be seen in the TEM image. Additionally, the nanoparticle catalyst that constituted of almost spherical dark spots was well distributed in the MSN support with very little agglomeration, which demonstrates that MSN indeed has a vital role in inhibiting the agglomeration of nanoparticles. This kind of improvement of the NiPd dispersion onto a silica-based support has been observed by Damyanova et al. [25].



**Figure 2.** Field emission scanning electron microscopy (FESEM) images of (A) MSN, (B) Pd black, (C) Pd-MSN, (D) Ni-MSN, (E) NiPd-C, and (F) NiPd-MSN electrocatalysts with a magnification 30,000 KX.



**Figure 3.** Mapping of (a) O nanoparticles, (b) Pd nanoparticles, (c) Ni nanoparticles, and (d) Si nanoparticles for NiPd-C (A) and NiPd-MSN (B) electrocatalysts.

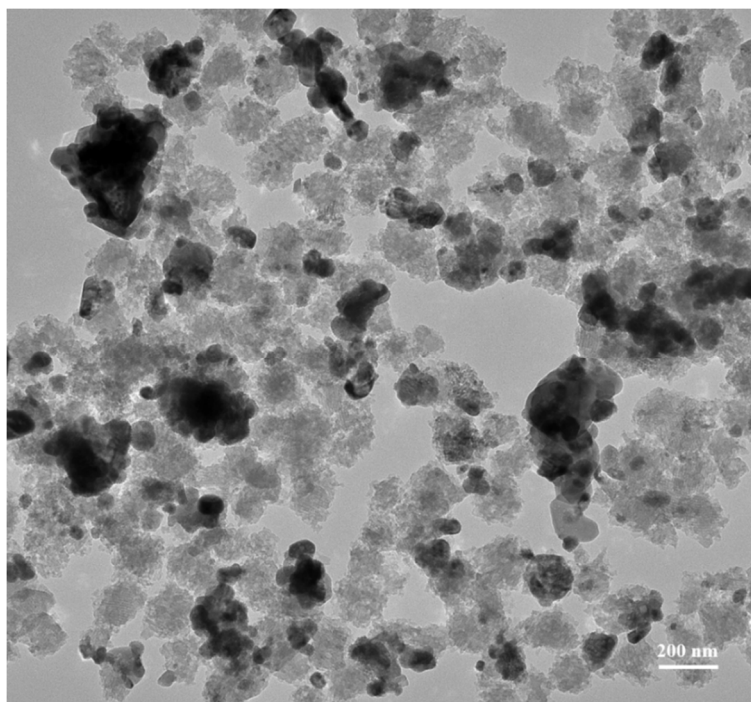


**Figure 4.** Transmission electron microscopy (TEM) images of NiPd-MSN electrocatalysts with magnification 30,000 KX.

To confirm the structural changes of composites, FTIR analysis of all catalysts with MSN as the support material was carried out and the outcomes are shown in Figure 5. All catalysts with MSN as support materials displayed similar FTIR spectra with typical patterns of MSN, consisting of bands at 457, 806, 970, 1093, 1641, and 3396  $\text{cm}^{-1}$ . From the IR peaks at the bands ascribed was Si–O–Si (457  $\text{cm}^{-1}$ ), Si–O–Si symmetric stretching (806  $\text{cm}^{-1}$ ), external Si–OH groups (970  $\text{cm}^{-1}$ ), Si–O–Si asymmetric stretching (1093  $\text{cm}^{-1}$ ), water molecules retained by siliceous materials (1641  $\text{cm}^{-1}$ ), and –OH stretching (3393  $\text{cm}^{-1}$ , broad) [26–28]. The relative intensity of the IR bands for transmittance was different, possibly due to the different morphology of all catalyst composites [23].

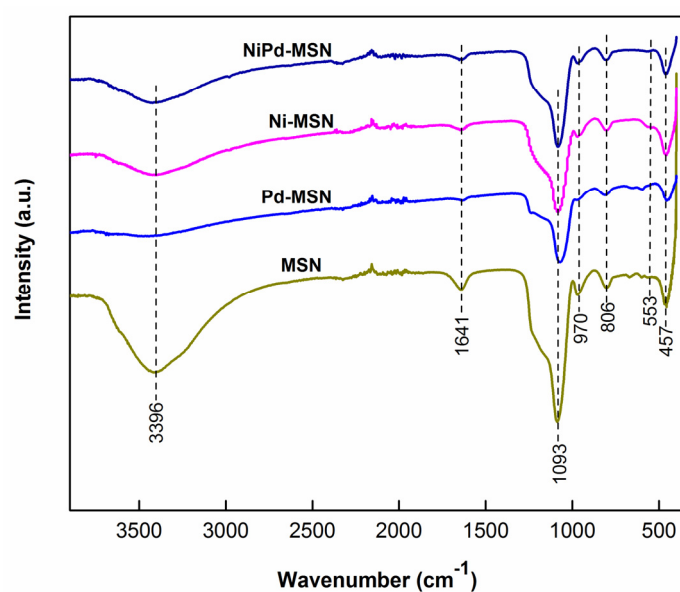


**Figure 5.** Fourier transform infrared (FTIR) spectra of MSN, Pd-MSN, Ni-MSN, and NiPd-MSN electrocatalysts.

The N<sub>2</sub> adsorption–desorption isotherms were used to study the changes in the pore structure of catalysts upon the addition of different supports of the NiPd–C and NiPd–MSN electrocatalysts, and the results are shown in Figure 6. For both electrocatalysts, the isotherms showed a type IV profile and type H1 hysteresis loops (International Union of Pure and Applied Chemistry (IUPAC) classification). The NiPd–MSN electrocatalyst presented a clear and sharp adsorption step than the NiPd–C electrocatalyst at relative pressure range  $P/P_0 = 0.8–1.0$ , and describe the characteristics of the existence of materials with mesoporous structure. Materials with a mesoporous structure showed good morphological stability and high catalyst active sites due to an increase in adsorption volume, indirectly increasing the electrocatalytic activity [29]. The textural properties for MSN, NiPd–C, and NiPd–MSN such as total pore volume, average pore diameter, and surface area were analyzed using the BET analysis are presented in Table 1. The BET surface area of MSN, NiPd–MSN, and NiPd–C showed a decreasing order from 1001.8 to 14.4 m<sup>2</sup> g<sup>−1</sup>. The BET surface area for NiPd–MSN decreased drastically due to the loading of NiPd, where the pores of MSN were blocked by NiO and PdO nanoparticles. With the introduction of nickel and palladium nanoparticles, the mean surface area and pore volume of MSN decreased significantly, presumably due to desilication, followed by isomorphous substitution of Ni and Pd ions into the silica network to form a bimodal pore structure [28]. The metal dispersion on the catalyst surface was influenced by the high surface area of the support. Nevertheless, the surface area of the BET does not represent the entire electrocatalytic surface area; electrochemical analysis is required to obtain the active surface area. The pore diameter of NiPd–MSN electrocatalyst was larger compared with the NiPd–C electrocatalyst. Small pores are inadequate as the pores in catalysts are typically filled with gaseous materials. Therefore, it will produce a liquid-sealing effect when the catalyst was used in liquid conditions [30]. Then, the gas in the pores is sealed and no other species can enter the pores. Thus, the alcohols (fuel) find it difficult to enter and leave from these pores. In contrast, the bigger size of the pore diameter is more promising for the mass transfer in the alcohol.

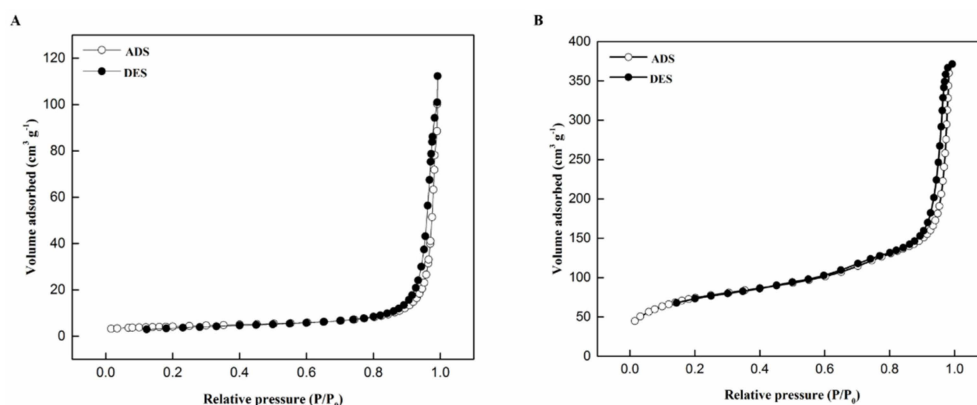


**Figure 6.** N<sub>2</sub> adsorption–desorption isotherm plots of the (A) NiPd–C and (B) NiPd–MSN electrocatalysts.

**Table 1.** Brunauer–Emmet–Teller (BET) analysis results for MSN, NiPd–C, and NiPd–MSN.

Catalyst	$S_{\text{BET}}$ (m <sup>2</sup> g <sup>−1</sup> )	$V_{\text{Total}}$ (cm <sup>3</sup> g <sup>−1</sup> )	$D_{\text{Pore}}$ (nm)
MSN	1001.8	0.813	3.25
NiPd–C	14.4	0.137	3.82
NiPd–MSN	270.8	0.532	7.85

X-ray photoelectron spectroscopy (XPS) was utilized to identify the chemical state, elemental composition, and elemental electronic state that exists within a material. Figure 7A shows a wide XPS scan from NiPd–MSN, which demonstrated the Pd, Ni, O, and Si peaks. These results correlated well with the energy dispersive X-ray (EDX) measurements. The elemental composition was divided into

3.8% Pd, 3.5% Ni, 61.0% O, and 31.7% Si. During the preparation process, the ratio of Ni to Pd used was 1.5:1. However, the actual ratio observed in XPS was 1:1. The content of the O element was 61.0%, which was abundant in the NiPd-MSN catalyst. The O 1s spectrum was deconvoluted into four peaks with the binding energy of 530.1, 531.2, 532.2, 533.1, 534.1, 535.0, and 537.0 eV, corresponding to the NiO, PdO, O-H, SiO<sub>2</sub>, H<sub>2</sub>O, Ni-OH, and Pd-OH, respectively (Figure 7B) [31–35].

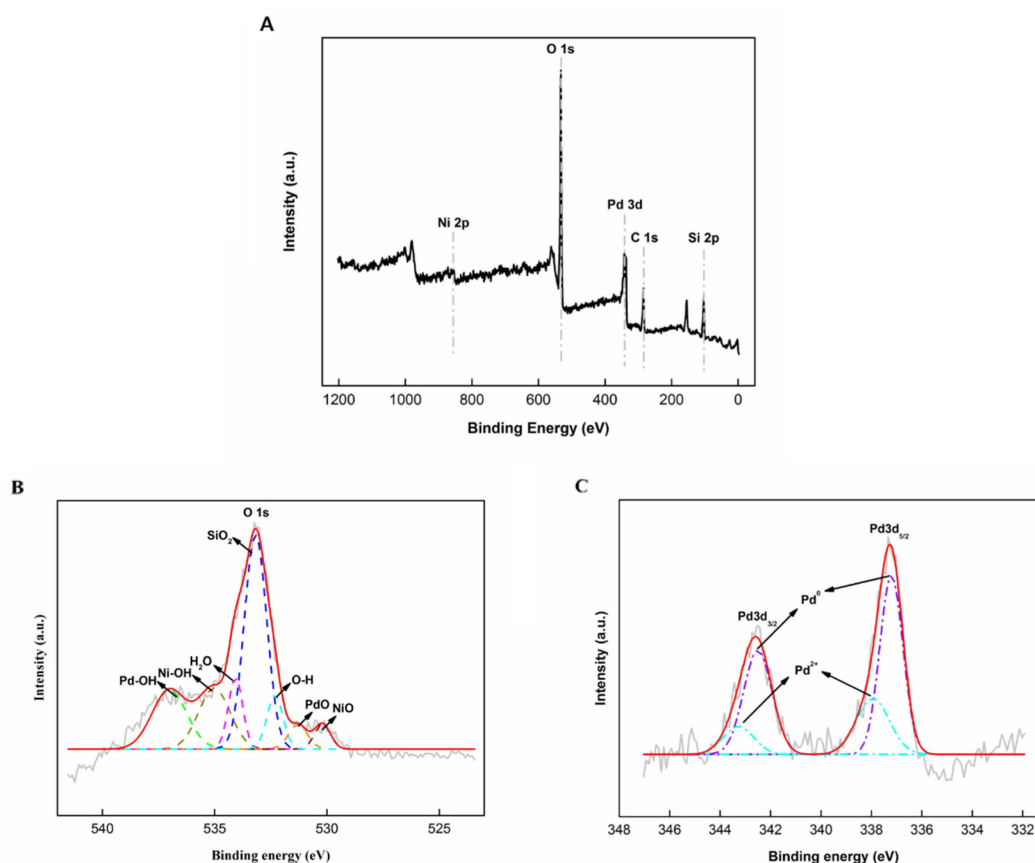


**Figure 7.** X-ray photoelectron spectroscopy (XPS) spectra of wide scan (A), O 1s (B), and Pd 3d (C) of the NiPd-MSN catalyst.

Figure 7C shows the XPS spectra of Pd3d of NiPd-MSN. The Pd3d spectra displayed a doublet at 342.6 and 337.3 eV, comprising a high-energy band (Pd3d<sub>3/2</sub>) and a low-energy band (Pd3d<sub>5/2</sub>), respectively. The Pd3d spectra exhibited two Pd states in the hybrid: one is a governed Pd<sup>0</sup> at a couple of peaks at 337.2 and 342.5 eV, and two is the 2+ oxidation state of Pd at the double binding energies of 337.9 and 343.3 eV [36]. This finding indicates that the metallic state of Pd exists. For the Pd3d<sub>3/2</sub> and Pd3d<sub>5/2</sub> spectra, corresponding to metallic Pd, the binding energy at 337.2 eV and 342.6 eV were assigned to the 30.25% and 42.09% species, respectively.

## 2.2. Electrochemical Characterization

### 2.2.1. Cyclic Voltammetry Testing

The cyclic voltammograms (Figure 6A) demonstrate the behavior of the Pd black, Pd-MSN, Ni-MSN, NiPd-C, and NiPd-MSN electrocatalysts at a scan rate of 50 mV s<sup>-1</sup> in the potential range from -1.0 V and 0.6 V vs. Ag/AgCl. On the anodic sweep for NiPd-MSN and NiPd-C, it is feasible to detect two main electrochemical techniques: hydrogen adsorption (from -0.85 V to -0.75 V vs. Ag/AgCl), and adsorbed hydrogen oxidation of Pd to PdO, while the possible potential region of Pd oxidizing to PdO remains unclear in alkaline conditions [18]. Nevertheless, the formation of PdO has suggested forms at more positive potentials. In the cathodic sweep, it is feasible to notice the reduction of PdO to

Pd peak (around  $-0.4$  to  $-0.2$  V vs. Ag/AgCl) for NiPd-MSN, while the reduction of PdO to the Pd peak (around  $-0.5$  to  $-0.4$  V vs. Ag/AgCl) for NiPd-C. Even though it had similar voltametric profiles, there were subtle differences in each voltammogram for methanol electrooxidation and adsorption in essential regions. The NiPd-MSN electrocatalyst shifted to a more positive potential compared to the NiPd-C electrocatalyst, which attributed to the synergy between Ni and Pd nanoparticles. Additionally, it indicates that the incorporation of Ni in Pd inhibits the chemisorption of OH on the Pd sites [16]. Due to the hydrogen penetration into all electrocatalysts, the electrochemical active surface areas (ECSAs) of all the samples was determined by the charge of the PdO to Pd reduction region and are tabulated in Table 2. An electrocatalyst's catalytic activity is known to be dependent on their ECSA. The ECSA for all the samples was determined via the following equation:

$$\text{ECSA} = \frac{Q}{S \cdot W_{\text{Pd}}} \quad (1)$$

where Q is the charge for the PdO reduction in coulomb ( $\mu\text{C}$ ); S is the proportionality constant used to relate charge over the area ( $405 \mu\text{C cm}^{-2}$ ) to associate the charge with the area; and  $W_{\text{Pd}}$  is the Pd loading on the electrode [37]. NiPd-MSN displayed the highest active surface area of Pd with  $19.53 \text{ m}^2 \text{ g}^{-1}_{\text{Pd}}$ . This result could be due to the smaller size of particles that has been observed in FESEM analysis (see Figure 2F). Similarly, as presented in Figure 8A, Pd black, Pd-MSN, and NiPd-C exhibited an ECSA of 14.95, 8.37,  $14.5 \text{ m}^2 \text{ g}^{-1}_{\text{Pd}}$ , respectively. The remarkable enhancement in ECSA of NiPd-MSN is attributed to the uniform dispersion NiPd catalysts on the large surface area of MSN as illustrated by the BET analysis in Table 1. Ni promotes anti-poisoning properties of NiPd catalysts due to its oxophilic nature, similar to Ru. It is capable of producing  $\text{OH}_{\text{ads}}$  at a lower potential and promotes the oxidative desorption of the intermediate products, thereby improving both the catalytic activity and stability of Pd catalysts [38].

**Table 2.** Summary of the electrochemical characterization of Pd black, Pd-MSN, Ni-MSN, NiPd-C and NiPd-MSN electrocatalysts.

Electrocatalyst	ECSA ( $\text{m}^2 \text{ g}^{-1}$ )	Onset Potential (V)	Oxidation Peak Current, $I_{\text{F}}$ ( $\text{mA mg}^{-1}_{\text{Pd}}$ )	Reduction Peak Current, $I_{\text{B}}$ ( $\text{mA mg}^{-1}_{\text{Pd}}$ )	$I_{\text{F}}/I_{\text{B}}$ Ratio
Pd black	14.95	$-0.40$	261.60	90.58	2.88
Pd-MSN	8.37	$-0.25$	371.90	106.95	3.47
Ni-MSN	NA	$-0.45$	208.55	88.32	2.36
NiPd-C	14.50	$-0.30$	637.59	150.88	4.22
NiPd-MSN	19.53	$-0.52$	657.03	175.39	3.74

The electrocatalytic activity of the NiPd-MSN electrocatalysts toward MOR using 1 M methanol in 1 M NaOH was tested using a cyclic voltammogram (Figure 8B). The anodic peak current density in the forward sweep is associated with the oxidation of freshly chemisorbed species originating from methanol adsorption [39]. The anodic peak current density in the backward sweep is ascribed to the removal of CO and other adsorbed intermediates incompletely oxidized in the forward sweep [40]. The measurements of anodic peak current on the forward sweep illustrate the electrocatalytic activity of the electrocatalysts for methanol electrooxidation. In terms of specific activity, the NiPd-MSN catalyst produced  $24.6 \text{ mA cm}^{-2}$ , which is greater than in the work of Tan et al. [18], and achieved a peak current of  $19.8 \text{ mA cm}^{-2}$  for palladium-nickel supported on exfoliated graphene oxide (PdNi/EGO). It should be noted that the noteworthy improvement of the electrocatalytic activity of NiPd-MSN toward MOR was attributed to the higher electrocatalyst active surface area on the MSN support and probably enhanced the synergistic effect of both metal particles. It is also believed that the enhanced synergistic effect between PdO and NiO was caused by the higher dispersion and improved support-catalyst interaction of the catalyst [14]. Mass activity (normalized by equivalent mass of Pd) is an important parameter to determine the possible application of electrocatalysts. As displayed in

Figure 8B, the mass activity of NiPd-MSN was the highest at  $657.03 \text{ mA mg}^{-1}$ , compared with Pd black, NiPd-C, Pd-MSN, and Ni-MSN, which were 261.60, 637.59, 371.90, and  $208.55 \text{ mA mg}^{-1}$ , respectively. Through the comparison, it further confirmed that the combination of Ni and Pd is vital to improve the electrocatalytic activity. Hence, it is reasonable to believe that the Ni sites in the electrocatalyst should play a significant active role during the process of MOR, while the Pd could act as a promoter. The mass activity for NiPd-MSN showed that it is comparable with other PdNi-based catalyst studies. As an example, Zhang et al. [41] reported that  $\text{Pd}_2\text{Ni}_3/\text{C}$  had a mass activity of  $544.22 \text{ mA mg}^{-1}$ , which was significantly lower than in this study. Thus, this proved that the electronic properties of Ni were changed after the addition of Pd and the unique structure of the support MSN seems to make the electrocatalysts have high mass activity and offer high performance for MOR [38]. As for NiPd-MSN, two separate oxidation peaks at  $-0.19$  and  $-0.15 \text{ V}$  are observable. The first oxidation peak is still recognizable as a plateau. This discovery suggests that two split reactions are involved for methanol oxidation on the bimetallic electrocatalyst site, or that the same reactions occur in a different location [42]. As NiPd-C does not exhibit this plateau, it is again implied that NiPd-MSN inherits electrochemical characteristics of both metals with a strong synergistic effect. This result is analogous to the findings made for measurements in a NaOH solution.

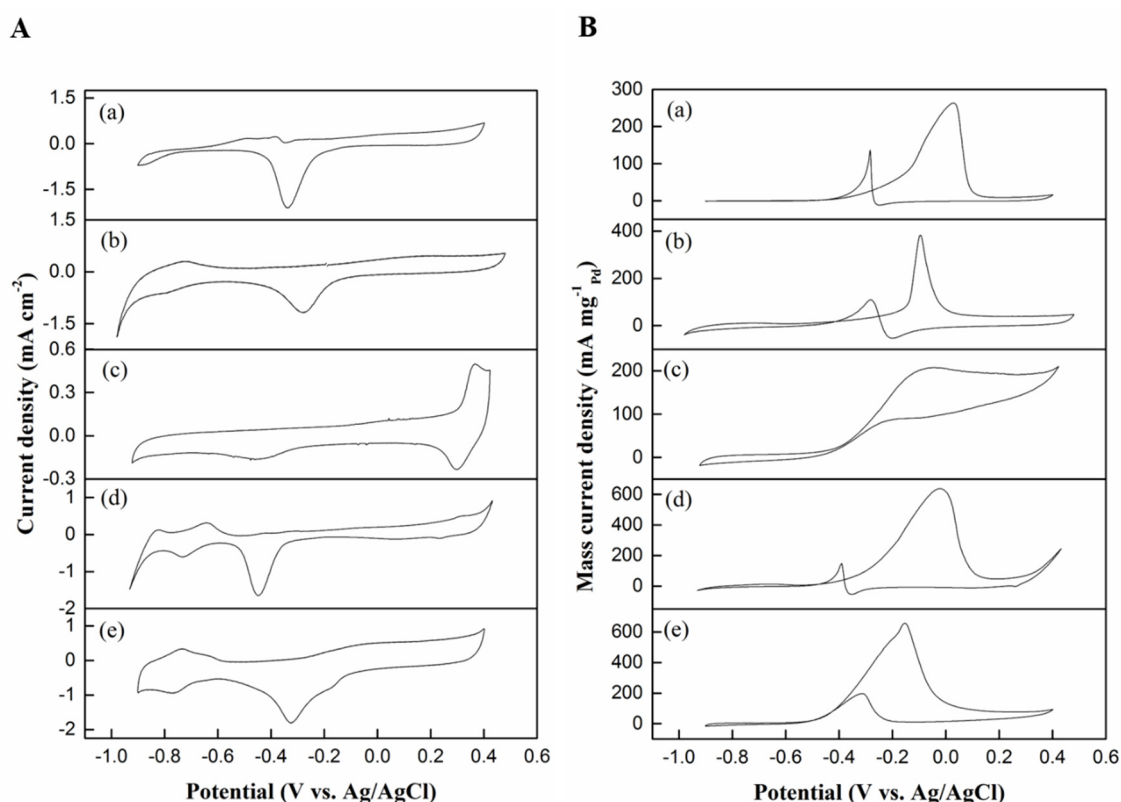


**Figure 8.** Cyclic voltammograms of (a) Pd black, (b) Pd-MSN, (c) Ni-MSN, (d) NiPd-C, and (e) NiPd-MSN electrocatalysts in 1 M NaOH (A) and 1 M NaOH + 1 M  $\text{CH}_3\text{OH}$  (B) with a scan rate 50 mV/s.

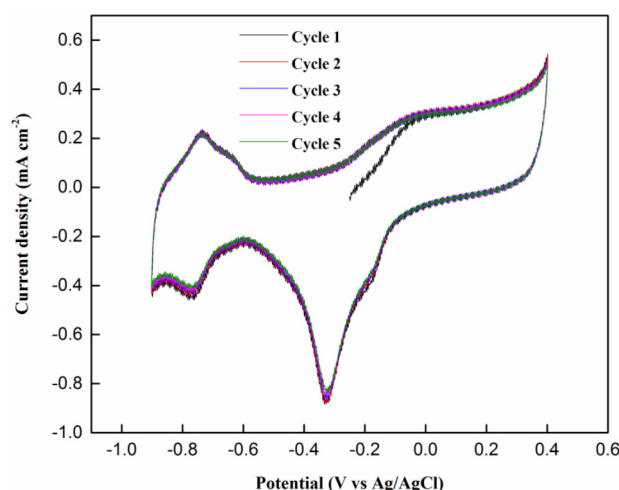
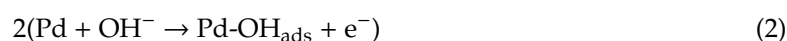
To further clarify the catalytic performance of the electrocatalysts toward MOR, the poisoning tolerance was evaluated. The forward anodic peak current (IF) to the backward anodic peak current (IB) ratio, IF/IB, can be employed to evaluate the tolerance to accumulated CO and other adsorbed species [43]. A higher IF/IB ratio generally implies a more effective removal of CO and other adsorbed intermediates on the electrocatalyst surface during the anodic scan [36]. As calculated, the IF/IB ratios of the Pd black, Pd-MSN, Ni-MSN, NiPd-C, and NiPd-MSN were 2.88, 3.47, 2.36, 4.22, and 3.74, respectively, as listed in Table 2. NiPd-C demonstrated the highest IF/IB value, indicating that in the

forward scan, more intermediate carbonaceous species were oxidized to CO<sub>2</sub> on its surface compared with other electrocatalysts [44]. Nonetheless, the NiPd–C electrocatalyst exhibited a lower mass activity toward methanol electrooxidation compared to the NiPd–MSN electrocatalyst by the observations above-mentioned. Additionally, the NiPd–C electrocatalyst possesses the highest overpotential for electrooxidation of methanol, as listed in Table 2. These suggest that this catalyst is inadequate for application. It is noteworthy that the I<sub>F</sub>/I<sub>B</sub> value of NiPd–MSN was higher than that of Pd black, signifying that MSN as a catalyst support can improve the tolerance to the CO<sub>ads</sub> intermediate species. In Table 3, the performance of the synthesized NiPd–C and NiPd–MSN electrocatalysts is compared with the other Pd-based electrocatalysts from previous studies.

**Table 3.** Comparison of the Pd-based electrocatalysts' performance with the previous study.

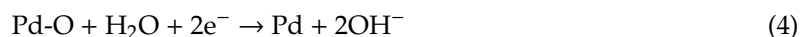
Electrocatalyst	ECSA (m <sup>2</sup> g <sup>-1</sup> )	Onset Potential (V)	Forward Peak Current, I <sub>F</sub> (mA mg <sup>-1</sup> )	I <sub>F</sub> /I <sub>B</sub> Ratio	Reference
Pd–NiO <sub>x</sub> –P/C	5.76	−0.48	364.00	1.52	[45]
Pd–4–Ni foam	NA	−0.562	180.8	NA	[46]
PdNi ND	22.02	−0.095	467.36	NA	[47]
Pd–NiO/C	NA	−0.46	248.00	0.57	[15]
Pd <sub>2</sub> Ni <sub>3</sub> /C	32.90	−0.75	544.22	1.72	[41]
NiPd–C	14.50	−0.30	637.59	4.22	This study
NiPd–MSN	19.53	−0.52	657.03	3.74	This study

Figure 9 shows the repeated five cycles of CV profiles for the NiPd–MSN electrocatalyst in 1.0 M NaOH. This experiment was carried out to confirm that the PdO was reduced to Pd after five cycles during the reaction. The anodic reactions at region −0.2 to 0.4 V in the forward scan were linked with the formation of the PdO layer on the catalyst surface [48–50]. Equations (2) and (3) can be described as the corresponding reactions [48]:



**Figure 9.** Cyclic voltammograms of the NiPd–MSN electrocatalysts in 1 M NaOH with a scan rate of 50 mV/s for five cycles.

The cathodic peak at region  $-0.5$  to  $-0.1$  V in the repeated CV was due to the reduction of PdO formed during the anodic scan, as shown in Equation (4):



From this reaction mechanism, it can be concluded that PdO was reduced to Pd after five cycles. This is because all the peaks were not shifted and hardly changed, but only decreased slightly in terms of current density.

Figure 10 shows the cyclic voltammograms of the NiPd-MSN electrocatalyst for MOR during the first five cycles. The cyclic voltammograms for NiPd-MSN in the forward scan displayed a slight decrease as the number of cycles increased from one to three. Later, the current density in the forward sweep was maintained at nearly constant. This happens as a significant quantity of PdO and carbonaceous intermediates have accumulated on the surface with repeated cycling. The PdO that formed blocked the active sites and the peak current forward scan decreased and the steady-state was observed [51]. The mechanism of methanol electrooxidation in alkaline media can be represented by Equations (5)–(9):

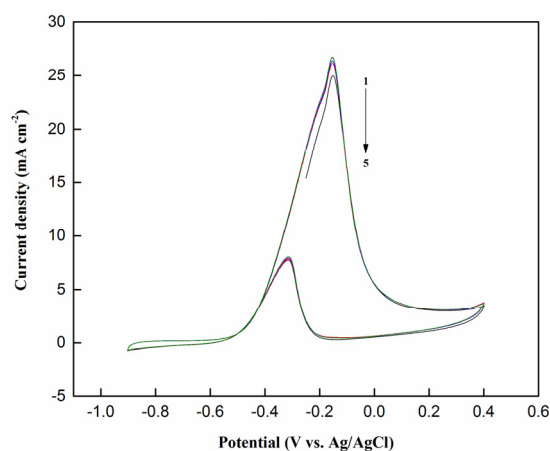
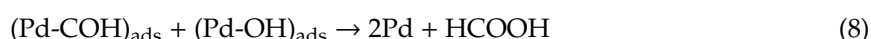
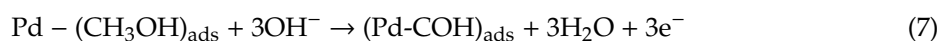


**Figure 10.** Cyclic voltammograms of NiPd-MSN electrocatalysts in 1 M NaOH + CH<sub>3</sub>OH with a scan rate of 50 mV/s for five cycles.

### 2.2.2. Tafel Slope Analysis

The measurements of linear sweeping voltammetry were performed as demonstrated in Figure 11 to identify the onset potential of methanol electrooxidation on the catalysts, as listed in Table 2. The methanol electrooxidation onset potential on the NiPd-MSN electrocatalyst was lower than that of the other investigated catalysts, suggesting that MSN can practically reduce the overpotential in methanol electrooxidation reaction. This result demonstrates that NiPd-MSN is easier for the methanol electrooxidation reaction that would take place on it compared with other electrocatalysts, as described in the literature where the lower onset potential is associated with the C–H bonds breaking and following the removal of intermediates by oxidation with OH<sub>ads</sub> [52,53]. Additionally, to introduce a Tafel plot, the LSV data were derived, where the reaction rate of the electrochemical was correlated with the overpotential.

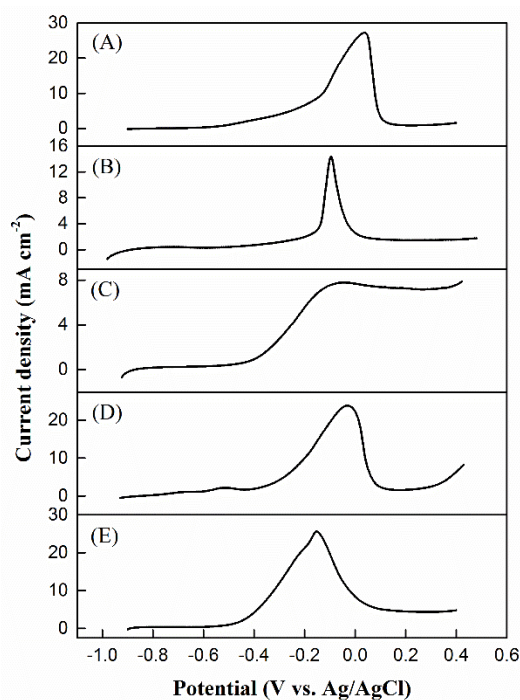


**Figure 11.** Linear sweep voltammograms of (A) Pd black, (B) Pd-MSN, (C) Ni-MSN, (D) NiPd-C, and (E) NiPd-MSN electrocatalysts in 1 M NaOH + 1 M CH<sub>3</sub>OH with the scan rate of 50 mV/s.

Tafel plots are capable of evaluating and determining the anodic slopes of the Tafel plot ( $b_a$ ) to compare the kinetic of the Pd black, NiPd-C, and NiPd-MSN electrocatalysts toward MOR. Data plot extraction is tabulated in Table 4, and the specified Tafel slope was extracted in the low potential range by plotting the overpotential,  $\eta$ , against the logarithm of current density;  $\log I$  is presented in Figure 12. It is stated that the CO<sub>ads</sub> adsorption is independent of the potential and the kinetics of MOR within such a potential range, and is calculated by the OH<sup>-</sup> adsorption on the electrode surface [54]. Despite this, NiPd-MSN had the lowest slope (200 mV dec<sup>-1</sup>) compared with the other electrocatalysts. The gradual Tafel slope demonstrates the fast kinetics of charge-transfer toward MOR. These results show that, due to the bifunctional mechanism, MSN addition into NiPd could produce the highest catalytic activity and shifted the onset potential toward the negative potentials [55].

**Table 4.** Data extraction from the Tafel plot.

Electrocatalyst	Tafel Slope, $b_a$ (mV dec <sup>-1</sup> )	Ionic Exchange Current Density, $j_0$ (mA cm <sup>-2</sup> )	Standard Deviation, R <sup>2</sup>
Pd black	440	0.051	0.995
NiPd-C	331	0.388	0.993
NiPd-MSN	201	0.398	0.989

By extrapolating the Tafel line to the point where the overpotential is equal to zero, the ionic exchange current density,  $j_0$  can be obtained. The ionic exchange current density is recognized as the catalytic activity explainer [56]. It can be proven from the Tafel plot in Figure 10 that the ionic exchange current density for NiPd-MSN was greater than that of NiPd-C and Pd black. As reported in the previous literature, the Pd content in the electrocatalyst affects the value of the ionic exchange current density, which is attributed to the incorporation of Pd atoms into the catalyst, leading to a dilution of catalytic Ni surface sites [57]. These data imply that the NiPd-MSN electrocatalyst had the best electrocatalytic performance for methanol electrooxidation in alkaline media in terms of lower onset potential and higher  $j_0$  compared with other electrocatalysts, and the values are given in Table 4.

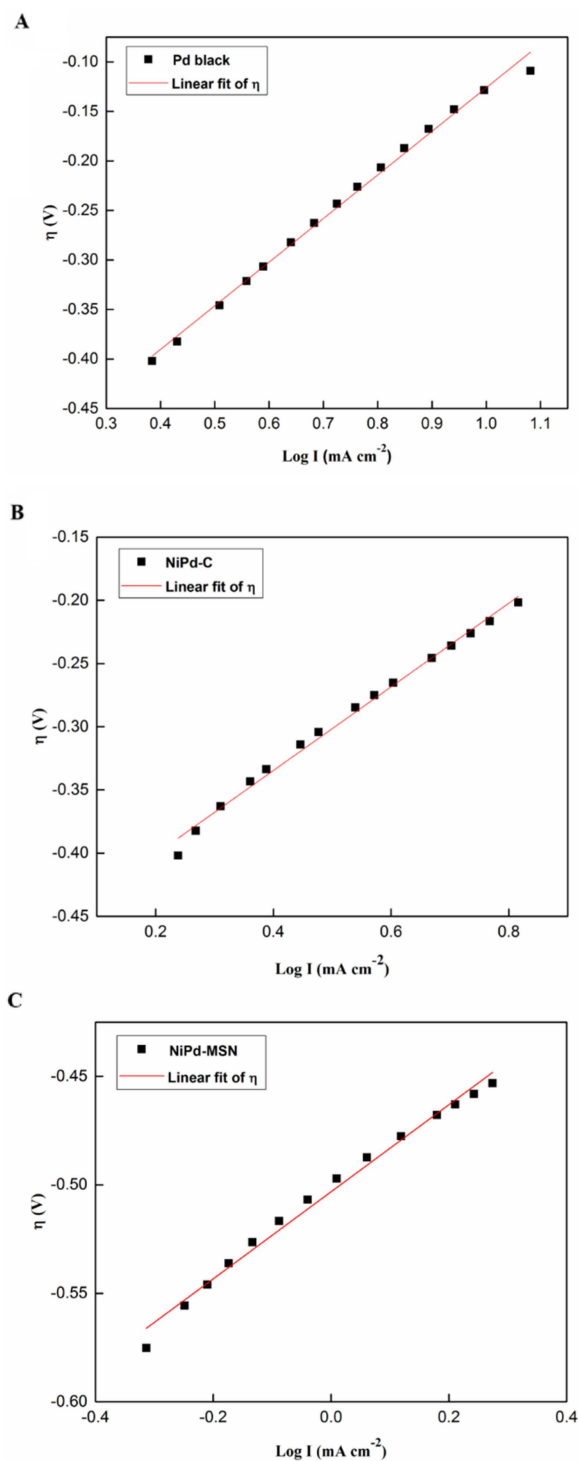


**Figure 12.** Tafel plot of (A) Pd black, (B) NiPd-C, and (C) NiPd-MSN electrocatalysts.

### 2.2.3. Chronoamperometry Testing

Figure 13 displays the chronoamperometry curves for methanol oxidation with Pd black, Pd-MSN, Ni-MSN, NiPd-C, and NiPd-MSN electrocatalysts achieved at room temperature using 1.0 M methanol in 1.0 M NaOH with a constant potential of  $-0.20$  V vs. Ag/AgCl for 3600 s. The tolerance to poisoning by intermediate species, activity, and stability toward MOR of the prepared electrocatalysts can be determined through this test. In all tests, the peak current attained a stable form and the stability of the electrocatalyst could be determined. It is worth noting that NiPd-MSN electrocatalysts have a greater mass activity toward methanol electrooxidation, in comparison to other electrocatalysts,

despite displaying a rapid current decay at the initial period, possibly resulting from the formation of intermediates and CO-like species adsorption on the Pd or because of the deactivation of their catalytic sites [18,36]. It can be observed that the limiting current of the NiPd-MSN over the entire period was higher than other electrocatalysts, indicating improved stability. The NiPd-MSN electrocatalysts retained 61% of its maximum current generated which the highest compared with Pd black (48% retention), Pd-MSN (31% retention), Ni-MSN (8% retention), and NiPd-C (53% retention). Thereby, it is implied that the synergistic effects from adding Ni to Pd are in charge of the lower poisoning rate [58]. Furthermore, it demonstrates that MSN as the support was an improved replacement for carbon black support, where the mesoporous structure of MSN can enhance the overall surface area and active reaction site on the electrocatalyst surface area.

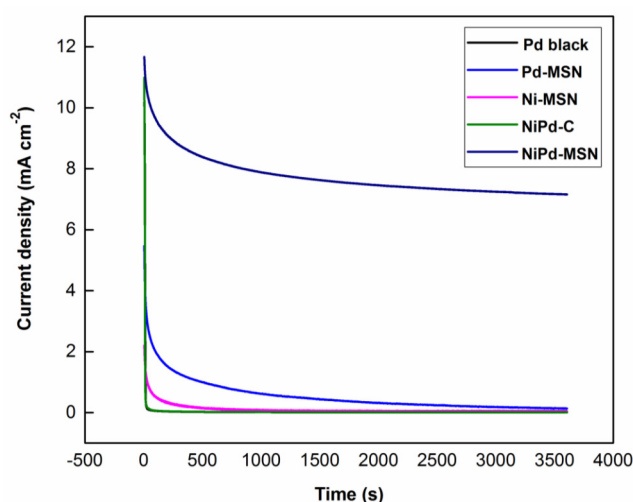


**Figure 13.** Chronoamperometry of Pd black, Pd-MSN, Ni-MSN, NiPd-C, and NiPd-MSN electrocatalysts in 1 M NaOH + 1 M MeOH at the potential of  $-0.2$  V.

### 3. Materials and Methods

#### 3.1. Chemicals and Reagents

For the synthesis of MSN, cetyltrimethylammonium bromide (CTAB), ethylene glycol (EG), tetraethyl orthosilicate (TEOS), and 3-aminopropyl triethoxysilane (APTES) were purchased from Merck (Darmstadt, EMD, Germany). Ethanol and ammonia solution ( $\text{NH}_4\text{OH}$ ) were bought from R&M, Malaysia. The aqueous nickel nitrate ( $\text{Ni}(\text{NO}_3)_2 \cdot 6\text{H}_2\text{O}$ ) and palladium chloride ( $\text{PdCl}_2\text{H}_4\text{O}_2$ ) precursor that was used to synthesize as the electrocatalyst were supplied from Sigma Aldrich (St. Louis, MO, USA). Additionally, graphite powder used in electrode preparation was supplied from Sigma Aldrich (St. Louis, MO, USA). 2-propanol and methanol solutions were obtained from Merck (Darmstadt, EMD, Germany) and a 5 wt.% Nafion solution was purchased from DuPont, USA, and the sodium hydroxide pellet (NaOH) was supplied from Macron Fine Chemical<sup>TM</sup>. Deionized water was used throughout the experiment. All the chemicals were of analytical grade and used without further purification.

#### 3.2. Synthesis of Mesostructured Silica Nanoparticle (MSN)

MSNs were synthesized using the sol-gel and co-condensation method according to the previous studies [27,28]. Briefly, in 720 mL of DI water, CTAB surfactant (4.68 g), EG solvent (120 mL), and  $\text{NH}_4\text{OH}$  solution (29 mL) were dissolved. After approximately 30 min of vigorous stirring at 323 K, TEOS (5.7 mL) and APTES (1.052 mL) were added to the clear solution. A white suspension mixture was produced and then for an additional 2 h, the solution was stirred at 353 K. The resulting mixture was allowed to rest for 24 h in the refrigerator until it completely separated into two layers. Then, the samples were accumulated for 10 min at 5000 rpm by centrifugation and washed five times

with DI water and absolute ethanol (1:1). The synthesized MSN was dried overnight at 383 K, followed by calcination for 3 h at 823 K to eliminate the surfactant.

### 3.3. Synthesis of NiPd–MSN

NiPd–MSN electrocatalysts were synthesized by the wet impregnation method [23,28]. The aqueous nickel nitrate ( $\text{Ni}(\text{NO}_3)_2 \cdot 6\text{H}_2\text{O}$ ) and palladium chloride ( $\text{PdCl}_2\text{H}_4\text{O}_2$ ) were impregnated on the support (MSN) at 353 K. Then, the sample was dried overnight at 383 K in the oven and then calcined for 3 h at 823 K in the air [14]. For comparison, all electrocatalysts were guaranteed with 30 wt.% metal loading while the ratio of Ni:Pd for both NiPd–C and NiPd–MSN was 3:2 [38,59].

### 3.4. Physical Characterization

Analysis of the X-ray diffractometer (XRD) was operated with a model Bruker D8 Advance at 40 kV with  $\text{CuK}\alpha$  radiation ( $\lambda = 0.15406 \text{ nm}$ ). In order to analyze the crystallinity and crystal phase of the electrocatalysts, the diffraction angle  $2\theta$  was measured from 20 to  $80^\circ$  while low angle XRD spectroscopy is typically used to determine the crystallographic of MSN phases [23,26,28]. The morphology of dispersion Ni on MSN was studied using field emission scanning electron microscopy (FESEM model no. SUPRA 55 VP). To determine the elements contained in the samples, we used EDX, which was attached to the FESEM. Fourier transform infrared (FTIR) spectroscopy (Perkin Elmer GX FTIR spectrometer) was carried out with a scan range of  $4000\text{--}400 \text{ cm}^{-1}$  to identify the chemical functional groups that exist in the samples. The catalyst was prepared using the KBr method, in which the catalysts and KBr matrix were mixed and then finely ground and put into pellet form with a ratio of 1 mg sample to 200 mg KBr. The electrocatalyst samples were analyzed by a nitrogen adsorption–desorption experiment at 77.35 K. The surface area values were determined using the Brunauer–Emmet–Teller (BET) theory, while pore volume and pore size distributions were determined using the Barret–Joyner–Halenda (BJH) method. A Kratos AXIS ULTRA DLD was used to analyze the X-ray photoelectron spectra (XPS).

### 3.5. Electrode Preparation

Electrocatalytic inks were produced by combining 15 mg of the catalyst and 15 mg of graphite powder with 100  $\mu\text{L}$  DI water, 100  $\mu\text{L}$  of 5 wt.% Nafion solution, and 800  $\mu\text{L}$  2-propanol. The resulting mixture was dispersed for 2 h in an ultrasonic bath. The resulting ink was then pipetted 2.5  $\mu\text{L}$  onto a glassy carbon electrode (GCE) surface, but before that, the electrode was well polished with 0.05  $\mu\text{m}$  alumina pastes followed by ultrasonic cleaning in DI water. The electrode was dried overnight before measurement.

### 3.6. Electrochemical Measurement

Electrochemical analysis of the electrocatalysts was performed by the Autolab (PGSTAT101) electrochemical workstation. Cyclic voltammetry (CV) in a conventional three-electrode cell was used to determine the electrocatalytic activity of the NiPd–MSN catalysts toward MOR. A glassy carbon electrode (GCE) with an area of  $0.07068 \text{ cm}^2$ , Ag/AgCl, and a Pt rod as the working electrode, the reference electrode, and the counter electrode, respectively. Before CV measurement was performed, a solution of 1.0 M NaOH in 1.0 M  $\text{CH}_3\text{OH}$  was bubbled with  $\text{N}_2$  saturated for 15 min to achieve the oxygen-free content. CV experiments were performed in a solution containing an electrolyte that was 1.0 M NaOH and 1 M  $\text{CH}_3\text{OH}$  as fuel at a scan rate of  $50 \text{ mVs}^{-1}$ , and the range of potentials was from  $-1.0$  to  $0.5 \text{ V}$  vs. Ag/AgCl at room temperature. Analogous tests were evaluated for measurements of chronoamperometry (CA). CA measurements were completed at  $-0.2 \text{ V}$  for 3600 s.

## 4. Conclusions

The MSN was successfully synthesized using the sol-gel method and used in the MOR as catalyst support for an anode catalyst, the NiPd composite. All catalysts were prepared by the wet impregnated

method. The prepared electrocatalysts including Ni-MSN, Pd-MSN, NiPd-MSN, and NiPd-C were tested in the electrochemical analysis, which were compared with one another. The results showed that NiPd-MSN had the highest mass activity ( $657.03 \text{ mA mg}^{-1}$ ), which was slightly higher than the NiPd-C. Additionally, it showed a greater stability toward MOR in the alkaline medium with 61% current retention and improved tolerance to the accumulation of carbonaceous species compared with other electrocatalysts. This excellent performance brought about the high dispersion of NiPd on the high surface area of MSN and the metal-support synergistic effect. Following these electrochemical and fuel cell properties, the NiPd-MSN electrocatalyst is a favorable anode material in DMFCs.

**Supplementary Materials:** The following are available online at <http://www.mdpi.com/2073-4344/10/11/1235/s1>, Figure S1: Particle size distribution histograms of (A) MSN and (B) NiPd-MSN catalysts, Figure S2: Cyclic voltammograms of MSN in 1 M NaOH (A) and 1 M NaOH + 1 M CH<sub>3</sub>OH (B) with a scan rate of 50 mV/s.

**Author Contributions:** Writing—original draft preparation, M.M.; Writing—review and editing, S.N.T., W.Y.W., A.M.Z., S.K.K., and K.L.L. All authors have read and agreed to the published version of the manuscript.

**Funding:** This research was funded by research project code no. PP-SELFUEL-2020 and the Ministry of Higher Education (MoHE), grant number FRGS/1/2019/STG01/UKM/03/1.

**Acknowledgments:** The authors acknowledge the financial support provided by research project code no. PP-SELFUEL-2020 and the Ministry of Higher Education, Malaysia through the Fundamental Research Grant Scheme FRGS/1/2019/STG01/UKM/03/1.

**Conflicts of Interest:** The authors declare no conflict of interest.

## References

1. Wang, Z.B.; Yin, G.P.; Shi, P.F. Effects of ozone treatment of carbon support on Pt-Ru/C catalysts performance for direct methanol fuel cell. *Carbon N. Y.* **2006**, *44*, 133–140. [[CrossRef](#)]
2. Yousaf, A.; Zaidi, S.J. Precious metal free Ni/Cu/Mo trimetallic nanocomposite supported on multi-walled carbon nanotubes as highly efficient and durable anode-catalyst for alkaline direct methanol fuel cells. *J. Electroanal. Chem.* **2018**, *823*, 98–105. [[CrossRef](#)]
3. Antolini, E.; Gonzalez, E.R. Alkaline direct alcohol fuel cells. *J. Power Sources* **2010**, *195*, 3431–3450. [[CrossRef](#)]
4. Geraldes, A.N.; Furtunato Da Silva, D.; Martins Da Silva, J.C.; Antonio De Sá, O.; Spinacé, E.V.; Neto, A.O.; Coelho Dos Santos, M. Palladium and palladium-tin supported on multi wall carbon nanotubes or carbon for alkaline direct ethanol fuel cell. *J. Power Sources* **2015**, *275*, 189–199. [[CrossRef](#)]
5. Debe, M.K. Electrocatalyst approaches and challenges for automotive fuel cells. *Nature* **2012**, *486*, 43–51. [[CrossRef](#)]
6. Zhao, Y.; Yang, X.; Tian, J.; Wang, F.; Zhan, L. Methanol electro-oxidation on Ni@Pd core-shell nanoparticles supported on multi-walled carbon nanotubes in alkaline media. *Int. J. Hydrogen Energy* **2010**, *35*, 3249–3257. [[CrossRef](#)]
7. Wang, Y.; Chen, W.; Pang, D.; Xu, Q. Methanol Electrooxidation Reaction in Alkaline Medium on Glassy Carbon Electrode Modified with Ordered Mesoporous Ni/Al<sub>2</sub>O<sub>3</sub>. *Int. J. Electrochem. Sci.* **2017**, *12*, 2194–2206. [[CrossRef](#)]
8. Lu, S.; Li, H.; Sun, J.; Zhuang, Z. Promoting the methanol oxidation catalytic activity by introducing surface nickel on platinum nanoparticles. *Nano Res.* **2017**, *11*, 2058–2068. [[CrossRef](#)]
9. Nieto-Monge, M.J.; Moliner, R. Palladium-nickel catalysts supported on different chemically-treated carbon blacks for methanol oxidation in alkaline media. *Int. J. Hydrogen Energy* **2016**, *41*, 19556–19569. [[CrossRef](#)]
10. Jin, C.; Sun, X.; Chen, Z.; Dong, R. Electrocatalytic activity of PdNi/C catalysts for allyl alcohol oxidation in alkaline solution. *Mater. Chem. Phys.* **2012**, *135*, 433–437. [[CrossRef](#)]
11. Amin, R.S.; Hameed, R.M.A.; El-khatib, K.M.; Youssef, M.E.; Elzatahry, A.A. Pt-NiO/C anode electrocatalysts for direct methanol fuel cells. *Electrochim. Acta* **2012**, *59*, 499–508. [[CrossRef](#)]
12. Zhou, Y.; Gao, Y.; Liu, Y.; Liu, J. High efficiency Pt-CeO<sub>2</sub>/carbon nanotubes hybrid composite as an anode electrocatalyst for direct methanol fuel cells. *J. Power Sources* **2010**, *195*, 1605–1609. [[CrossRef](#)]
13. Hu, F.; Chen, C.; Wang, Z.; Wei, G.; Kang, P. Mechanistic study of ethanol oxidation on Pd-NiO/C electrocatalyst. *Electrochim. Acta* **2006**, *52*, 1087–1091. [[CrossRef](#)]

14. Wang, M.; Liu, W.; Huang, C. Investigation of PdNiO/C catalyst for methanol electrooxidation. *Int. J. Hydrogen Energy* **2009**, *34*, 2758–2764. [[CrossRef](#)]
15. Ye, K.; Zhou, S.; Zhu, X.; Xu, C.; Kang, P. Stability analysis of oxide (CeO<sub>2</sub>, NiO, Co<sub>3</sub>O<sub>4</sub> and Mn<sub>3</sub>O<sub>4</sub>) effect on Pd/C for methanol oxidation in alkaline medium. *Electrochim. Acta* **2013**, *90*, 108–111. [[CrossRef](#)]
16. Liu, Z.; Zhang, X.; Hong, L. Physical and electrochemical characterizations of nanostructured Pd/C and PdNi/C catalysts for methanol oxidation. *Electrochem. Commun.* **2009**, *11*, 925–928. [[CrossRef](#)]
17. Li, N.; Sun, S.; Chen, S. Studies on the role of oxidation states of the platinum surface in electrocatalytic oxidation of small primary alcohols. *J. Electroanal. Chem.* **1997**, *430*, 57–67. [[CrossRef](#)]
18. Tan, J.L.; De Jesus, A.M.; Chua, S.L.; Sanetuntikul, J.; Shanmugam, S.; Tongol, B.J.V.; Kim, H. Preparation and characterization of palladium-nickel on graphene oxide support as anode catalyst for alkaline direct ethanol fuel cell. *Appl. Catal. A Gen.* **2017**, *531*, 29–35. [[CrossRef](#)]
19. Mao, Y.-H.; Chen, C.-Y.; Fu, J.-X.; Lai, T.-Y.; Lu, F.-H.; Tsai, Y.-C. Electrodeposition of nickel-copper on titanium nitride for methanol electrooxidation. *Surf. Coat. Technol.* **2018**, *350*, 949–953. [[CrossRef](#)]
20. Tang, D.; Zhang, L.; Zhang, Y.; Qiao, Z.A.; Liu, Y.; Huo, Q. Mesoporous silica nanoparticles immobilized salicylaldehyde cobalt complexes as high efficient catalysts for polymerization of 1,3-butadiene. *J. Colloid Interface Sci.* **2012**, *369*, 338–343. [[CrossRef](#)]
21. Jusoh, N.W.C.; Jalil, A.A.; Triwahyono, S.; Karim, A.H.; Salleh, N.F.; Annuar, N.H.R.; Jaafar, N.F.; Firmansyah, M.L.; Mukti, R.R.; Ali, M.W. Structural rearrangement of mesostructured silica nanoparticles incorporated with ZnO catalyst and its photoactivity: Effect of alkaline aqueous electrolyte concentration. *Appl. Surf. Sci.* **2015**, *330*, 10–19. [[CrossRef](#)]
22. Sazegar, M.R.; Jalil, A.A.; Triwahyono, S.; Mukti, R.R.; Aziz, M.; Aziz, M.A.A.; Setiabudi, H.D.; Kamarudin, N.H.N. Protonation of Al-grafted mesostructured silica nanoparticles (MSN): Acidity and catalytic activity for cumene conversion. *Chem. Eng. J.* **2014**, *240*, 352–361. [[CrossRef](#)]
23. Aziz, M.A.A.; Jalil, A.A.; Triwahyono, S.; Saad, M.W.A. CO<sub>2</sub> methanation over Ni-promoted mesostructured silica nanoparticles: Influence of Ni loading and water vapor on activity and response surface methodology studies. *Chem. Eng. J.* **2014**, *260*, 757–764. [[CrossRef](#)]
24. Zainoodin, A.M.; Kamarudin, S.K.; Daud, W.R.W. Electrode in direct methanol fuel cells. *Int. J. Hydrogen Energy* **2010**, *35*, 4606–4621. [[CrossRef](#)]
25. Damyanova, S.; Pawelec, B.; Arishtirova, K.; Fierro, J.L.G.; Sener, C.; Dogu, T. MCM-41 supported PdNi catalysts for dry reforming of methane. *Appl. Catal. B Environ.* **2009**, *92*, 250–261. [[CrossRef](#)]
26. Karim, A.H.; Jalil, A.A.; Triwahyono, S.; Sidik, S.M.; Kamarudin, N.H.N.; Jusoh, R.; Jusoh, N.W.C.; Hameed, B.H. Amino modified mesostructured silica nanoparticles for efficient adsorption of methylene blue. *J. Colloid Interface Sci.* **2012**, *386*, 307–314. [[CrossRef](#)]
27. Karim, A.H.; Jalil, A.A.; Triwahyono, S.; Kamarudin, N.H.N.; Ripin, A. Influence of multi-walled carbon nanotubes on textural and adsorption characteristics of in situ synthesized mesostructured silica. *J. Colloid Interface Sci.* **2014**, *421*, 93–102. [[CrossRef](#)]
28. Aziz, M.A.A.; Jalil, A.A.; Triwahyono, S.; Mukti, R.R.; Taufiq-Yap, Y.H.; Sazegar, M.R. Highly active Ni-promoted mesostructured silica nanoparticles for CO<sub>2</sub> methanation. *Appl. Catal. B Environ.* **2014**, *147*, 359–368. [[CrossRef](#)]
29. Pal, N.; Bhaumik, A. Mesoporous materials: Versatile supports in heterogeneous catalysis for liquid phase catalytic transformations. *RSC Adv.* **2015**, *5*, 24363–24391. [[CrossRef](#)]
30. Yan, Z.; Meng, H.; Kang, P.; Meng, Y.; Ji, H. Effect of the templates on the synthesis of hollow carbon materials as electrocatalyst supports for direct alcohol fuel cells. *Int. J. Hydrogen Energy* **2011**, *37*, 4728–4736. [[CrossRef](#)]
31. Wang, C.; Yang, F.; Yang, W.; Ren, L.; Zhang, Y.; Jia, X.; Zhang, L.; Li, Y. PdO nanoparticles enhancing the catalytic activity of Pd/carbon nanotubes for 4-nitrophenol reduction. *RSC Adv.* **2015**, *5*, 27526–27532. [[CrossRef](#)]
32. Jusoh, N.W.C.; Jalil, A.A.; Triwahyono, S.; Mamat, C.R. Tailoring the metal introduction sequence onto mesostructured silica nanoparticles framework: Effect on physicochemical properties and photoactivity. *Appl. Catal. A Gen.* **2015**, *492*, 169–176. [[CrossRef](#)]
33. Qi, T.; Sun, J.; Yang, X.; Yan, F.; Zuo, J. Effects of Chemical State of the Pd Species on H<sub>2</sub> Sensing Characteristics of PdO<sub>x</sub>/SnO<sub>2</sub> Based Chemiresistive Sensors. *Sensors* **2019**, *19*, 3131. [[CrossRef](#)]
34. Rodríguez, J.L.; Valenzuela, M.A.; Poznyak, T.; Lartundo, L.; Chairez, I. Reactivity of NiO for 2,4-D degradation with ozone: XPS studies. *J. Hazard. Mater.* **2013**, *262*, 472–481. [[CrossRef](#)]

35. Gomez-Bolivar, J.; Mikheenko, I.P.; Orozco, R.L.; Sharma, S.; Banerjee, D.; Walker, M.; Hand, R.A.; Merroun, M.L.; Macaskie, L.E. Synthesis of Pd/Ru bimetallic nanoparticles by *Escherichia coli* and potential as a catalyst for upgrading 5-hydroxymethyl furfural into liquid fuel precursors. *Front. Microbiol.* **2019**, *10*, 1276. [[CrossRef](#)]
36. Chao, L.; Qin, Y.; He, J.; Ding, D.; Chu, F. Robust three dimensional N-doped graphene supported Pd nanocomposite as efficient electrocatalyst for methanol oxidation in alkaline medium. *Int. J. Hydrogen Energy* **2017**, *42*, 15107–15114. [[CrossRef](#)]
37. Ting, L.; Shyuan, K.; Bakar, A.; Ramli, W.; Daud, W. Synthesis of silver/nitrogen-doped reduced graphene oxide through a one-step thermal solid-state reaction for oxygen reduction in an alkaline medium. *J. Power Sources* **2016**, *324*, 412–420. [[CrossRef](#)]
38. Shen, S.Y.; Zhao, T.S.; Xu, J.B.; Li, Y.S. Synthesis of PdNi catalysts for the oxidation of ethanol in alkaline direct ethanol fuel cells. *J. Power Sources* **2010**, *195*, 1001–1006. [[CrossRef](#)]
39. Chen, Z.; He, Y.C.; Chen, J.H.; Fu, X.Z.; Sun, R.; Chen, Y.X.; Wong, C.P. PdCu Alloy Flower-like Nanocages with High Electrocatalytic Performance for Methanol Oxidation. *J. Phys. Chem. C* **2018**, *122*, 8976–8983. [[CrossRef](#)]
40. Yahya, N.; Kamarudin, S.K.; Karim, N.A.; Basri, S.; Zanoodin, A.M. Nanostructured Pd-Based Electrocatalyst and Membrane Electrode Assembly Behavior in a Passive Direct Glycerol Fuel. *Nanoscale Res. Lett.* **2019**, *14*, 52. [[CrossRef](#)]
41. Zhang, Z.; Xin, L.; Sun, K.; Li, W. Pd-Ni electrocatalysts for efficient ethanol oxidation reaction in alkaline electrolyte. *Int. J. Hydrogen Energy* **2011**, *36*, 12686–12697. [[CrossRef](#)]
42. Jurzinsky, T.; Bär, R.; Cremers, C.; Tübke, J.; Elsner, P. Highly active carbon supported palladium-rhodium Pd X Rh/C catalysts for methanol electrooxidation in alkaline media and their performance in anion exchange direct methanol fuel cells (AEM-DMFCs). *Electrochim. Acta* **2015**, *176*, 1191–1201. [[CrossRef](#)]
43. Yahya, N.; Kamarudin, S.K.; Karim, N.A.; Masdar, M.S.; Loh, K.S.; Lim, K.L. Durability and performance of direct glycerol fuel cell with palladium-aurum/vapor grown carbon nanofiber support. *Energy Convers. Manag.* **2019**, *188*, 120–130. [[CrossRef](#)]
44. Zhao, Y.; Zhan, L.; Tian, J.; Nie, S.; Ning, Z. Enhanced electrocatalytic oxidation of methanol on Pd/polypyrrole-graphene in alkaline medium. *Electrochim. Acta* **2011**, *56*, 1967–1972. [[CrossRef](#)]
45. Kang, Y.; Wang, W.; Pu, Y.; Li, J.; Chai, D.; Lei, Z. An effective Pd-NiO<sub>x</sub>-P composite catalyst for glycerol electrooxidation: Co-existed phosphorus and nickel oxide to enhance performance of Pd. *Chem. Eng. J.* **2017**, *308*, 419–427. [[CrossRef](#)]
46. Niu, X.; Zhao, H.; Lan, M. Palladium deposits spontaneously grown on nickel foam for electro-catalyzing methanol oxidation: Effect of precursors. *J. Power Sources* **2016**, *306*, 361–368. [[CrossRef](#)]
47. Zheng, J.N.; He, L.L.; Chen, F.Y.; Wang, A.J.; Xue, M.W.; Feng, J.J. A facile general strategy for synthesis of palladium-based bimetallic alloyed nanodendrites with enhanced electrocatalytic performance for methanol and ethylene glycol oxidation. *J. Mater. Chem. A* **2014**, *2*, 12899–12906. [[CrossRef](#)]
48. Habibi, B.; Mohammadyari, S. Facile synthesis of Pd nanoparticles on nano carbon supports and their application as an electrocatalyst for oxidation of ethanol in alkaline media: The effect of support. *Int. J. Hydrogen Energy* **2015**, *40*, 10833–10846. [[CrossRef](#)]
49. Geraldine, A.N.; Da Silva, D.F.; Pino, E.S.; Da Silva, J.C.M.; De Souza, R.F.B.; Hammer, P.; Spinacé, E.V.; Neto, A.O.; Linardi, M.; Dos Santos, M.C. Ethanol electro-oxidation in an alkaline medium using Pd/C, Au/C and PdAu/C electrocatalysts prepared by electron beam irradiation. *Electrochim. Acta* **2013**, *111*, 455–465.
50. Xu, J.B.; Zhao, T.S.; Li, Y.S.; Yang, W.W. Synthesis and characterization of the Au-modified Pd cathode catalyst for alkaline direct ethanol fuel cells. *Int. J. Hydrogen Energy* **2010**, *5*, 3–10. [[CrossRef](#)]
51. Mukherjee, P.; Bagchi, J.; Dutta, S.; Bhattacharya, S.K. The nickel supported platinum catalyst for anodic oxidation of ethanol in alkaline medium. *Appl. Catal. A Gen.* **2015**, *506*, 220–227. [[CrossRef](#)]
52. Baronia, R.; Goel, J.; Tiwari, S.; Singh, P.; Singh, D.; Singh, S.P.; Singhal, S.K. Efficient electro-oxidation of methanol using PtCo nanocatalysts supported reduced graphene oxide matrix as anode for DMFC. *Int. J. Hydrogen Energy* **2017**, *42*, 3–12. [[CrossRef](#)]
53. Semasko, M.; Tamasauskaite-Tamasiunaite Kepeniene, V.; Balciunaite, A.; Vaiciuniene, J.; Drabavicius, A.; Norkus, E. Evaluation of Activity of Platinum-Ruthenium-Cobalt/Graphene Catalysts towards Methanol Oxidation. *ECS Trans.* **2015**, *68*, 55–62. [[CrossRef](#)]

54. Liang, Z.X.; Zhao, T.S.; Xu, J.B.; Zhu, L.D. Mechanism study of the ethanol oxidation reaction on palladium in alkaline media. *Electrochim. Acta* **2009**, *54*, 2203–2208. [[CrossRef](#)]
55. Ren, Y.; Zhang, S.; Li, H. Electro-oxidation of methanol on SnO<sub>2</sub>-promoted Pd/MWCNTs catalysts in alkaline solution. *Int. J. Hydrogen Energy* **2014**, *39*, 288–296. [[CrossRef](#)]
56. Abdullah, N.; Kamarudin, S.K. Novel Anodic Catalyst Support for Direct Methanol Fuel Cell: Characterizations and Single-Cell Performances. *Nanoscale Res. Lett.* **2018**, *13*, 90. [[CrossRef](#)]
57. Dinesh, B.; Saraswathi, R. Enhanced performance of Pt and Pt–Ru supported PEDOT–RGO nanocomposite towards methanol oxidation. *Int. J. Hydrogen Energy* **2016**, *41*, 13448–13458. [[CrossRef](#)]
58. Jurzinsky, T.; Kammerer, P.; Cremers, C.; Pinkwart, K.; Tübke, J. Investigation of ruthenium promoted palladium catalysts for methanol electrooxidation in alkaline media. *J. Power Sources* **2016**, *303*, 182–193. [[CrossRef](#)]
59. Qi, Z.; Geng, H.; Wang, X.; Zhao, C.; Ji, H.; Zhang, C.; Xu, J.; Zhang, Z. Novel nanocrystalline PdNi alloy catalyst for methanol and ethanol electro-oxidation in alkaline media. *J. Power Sources* **2011**, *196*, 5823–5828. [[CrossRef](#)]

**Publisher’s Note:** MDPI stays neutral with regard to jurisdictional claims in published maps and institutional affiliations.



© 2020 by the authors. Licensee MDPI, Basel, Switzerland. This article is an open access article distributed under the terms and conditions of the Creative Commons Attribution (CC BY) license (<http://creativecommons.org/licenses/by/4.0/>).